AGU100 ADVANCING EARTH AND SPACE SCIENCE

Geophysical Research Letters

Key Points:
- Distributions of temperature for an aquaplanet model are explained in terms of horizontal advection of temperature and other processes
- The shape of midlatitude distributions can be explained by horizontal advection, except in the upper and lower 10% of the distribution
- At each percentile, we decompose changes to the distributions into changes in the mean, in horizontal advection, and in other processes

Supporting Information:
- Supporting Information S1

Correspondence to:
M. Linz,
mlinz@seas.harvard.edu

A Framework for Understanding How Dynamics Shape Temperature Distributions

Marianna Linz[1,2] , **Gang Chen[3]** , **Boer Zhang[1]** , and **Pengfei Zhang[3]**

[1]School of Engineering and Applied Sciences, Harvard University, Cambridge, MA, USA, [2]Department of Earth and Planetary Sciences, Harvard University, Cambridge, MA, USA, [3]Department of Atmospheric and Oceanic Sciences, University of California, Los Angeles, Los Angeles, CA, USA

Abstract Understanding what physically sets the shape of temperature distributions will enable more robust predictions of local temperature with global warming. We derive the relationship between the temperature distribution shape and the advection of temperature conditionally averaged at each temperature percentile. This enables quantification of the shift of each percentile that is due to changes in the mean temperature, in horizontal temperature advection, and other processes (e.g., radiation and convection). We use this relationship to examine global model simulations in an idealized aquaplanet model with increasing carbon dioxide. Changes in the distribution with doubling and quadrupling of carbon dioxide are significant, and they are caused by different processes. We find that midlatitude temperature distributions can be explained mostly by the horizontal advection, except in the upper and lower 10% of the distribution.

1. Introduction

Observed (McKinnon et al., 2016; Rhines et al., 2017) and predicted (Tamarin-Brodsky et al., 2019) temperature changes with global warming are not simply an increase in the mean temperature but changes to the shape of the distribution as well. Variance changes are a balance between decreases in the meridional temperature gradient and possible changes to jet waviness advecting across that gradient (Alexander & Perkins, 2013). Skewness changes, meanwhile, are fundamental to changes in jet position (Linz et al., 2018). The shape of the temperature distribution is important for extremes (Loikith & Neelin, 2015); different shapes of local temperature distributions mean that on average, poorer countries will experience record-breaking extremes sooner than wealthier countries (Harrington et al., 2016). In their review paper, Hoskins and Woollings (2015) conclude that to understand climate change, research must focus on what atmospheric physics set the detailed shape of temperature distributions.

Many factors can influence extreme temperatures, including the large-scale atmospheric circulation, local thermodynamics, radiation, and smaller-scale effects. For current extreme heat events, studies have found that heat in different regions is driven by some combination of radiation, surface heat fluxes, horizontal temperature advection, and subsidence (Bieli et al., 2015; Quinting & Reeder, 2017; Zschenderlein et al., 2019). For future extreme heat events, changes to the moist thermodynamics are certain, and large-scale soil moisture changes might also be expected (e.g., Seneviratne et al., 2010). Meanwhile, trends in summertime circulation have tended toward a weaker circulation (Coumou et al., 2015) and an increase in wave patterns associated with heat waves (Mann et al., 2018).

In this paper, we focus on understanding the balance between large-scale temperature advection and diabatic processes in setting the shape of the temperature distribution, with the goal of understanding the underlying physics. In section 2, we present the conditional-averaging framework (cf. Norris et al., 2019 and Chen et al., 2019 for application to extreme precipitation). We use this framework in section 4 to examine an aquaplanet model (described in section 3) at different latitudes and with increased CO_2. In section 5, we demonstrate the decomposition of changes in the temperature distribution into different physical components. Finally, in section 6, we discuss implications and limitations of this study.

2. Using Conditional Means to Understand the Temperature Distribution

The time evolution of potential temperature, θ, can be described by

$$\frac{\partial \theta}{\partial t} = -\mathbf{v} \cdot \Delta \theta + \dot{\theta}, \tag{1}$$

where $\mathbf{v}$ is the wind vector, (u, v, ω), $\Delta \theta$ is the temperature gradient, and $\dot{\theta}$ denotes all other processes that can contribute to the temperature tendency (the diabatic processes).

Consider an ensemble of N realizations governed by the temperature-advection equation with different initial conditions. We will construct the temperature tendency as a function of the temperature distribution in the ensemble. The conditional mean of a variable X with respect to temperature θ can be written as

$$\langle X \rangle_\theta \equiv \frac{\sum_{i=1}^{N} \delta(\theta - \theta_i) X_i}{\sum_{i=1}^{N} \delta(\theta - \theta_i)} \tag{2}$$

where θ_i and X_i denote the values in the ith realization. The parameter $\delta()$ is a delta function that is related to the Heaviside function $\mathcal{H}()$ by $\delta(\theta) = \partial \mathcal{H}(\theta)/\partial \theta$.

Using the cumulative density function of θ

$$c(\theta) = \frac{1}{N} \sum_{i=1}^{N} \mathcal{H}(\theta - \theta_i), \tag{3}$$

one obtains the tendency of the cumulative density function as

$$\frac{\partial c}{\partial t}\big|_\theta = -\frac{1}{N} \sum_{i=1}^{N} \delta(\theta - \theta_i) \frac{\partial \theta_i}{\partial t} = -\frac{\partial c}{\partial \theta} \langle \frac{\partial \theta}{\partial t} \rangle_\theta, \tag{4}$$

where $\partial c/\partial \theta = \frac{1}{N} \sum_{i=1}^{N} \delta(\theta - \theta_i)$ is the probability distribution function (PDF) of θ.

For a given time t, θ is a monotonic function of the temperature percentile e in the ensemble. Thus, we make a coordinate transform from θ to the eth percentile of θ, $c = c(\theta(e, t), t)$. Noting $c = 100e$, then

$$\frac{dc}{dt}\big|_e = \frac{\partial c}{\partial t}\big|_\theta + \frac{\partial c}{\partial \theta}\big|_t \frac{\partial \theta}{\partial t}\big|_e = 0, \tag{5}$$

where the subscript is the variable held constant in the partial derivative. Thus, substituting with equations (4) and (1), the change in the eth percentile of θ is

$$\begin{aligned}
\frac{\partial \theta^e}{\partial t} \equiv \frac{\partial \theta}{\partial t}\big|_e &= -(\frac{\partial c}{\partial \theta})^{-1} \frac{\partial c}{\partial t}\big|_\theta \\
&= \langle \frac{\partial \theta}{\partial t} \rangle_{\theta^e} = -\langle \mathbf{v} \cdot \Delta \theta \rangle_{\theta^e} + \langle \dot{\theta} \rangle_{\theta^e}.
\end{aligned} \tag{6}$$

Intuitively, this makes sense; the tendency of temperature in the eth percentile is impacted by the processes occurring right at that percentile, both advection of temperature and other processes. This coordinate transformation from temperature to percentile is analogous to the transformations from potential vorticity to equivalent latitude or from potential temperature to equivalent pressure used to quantify transport and mixing in the atmosphere (Chen, 2013; Nakamura, 1995).

Now consider $\langle \dot{\theta} \rangle_{\theta^e}$, which includes all processes except temperature advection that contribute to the temperature tendency at the eth percentile. We can write the first-order Taylor series expansion in the form of a Newtonian relaxation (cf. Held & Suarez, 1994):

$$\langle \dot{\theta} \rangle_{\theta^e} \approx \langle \frac{-\theta^e + \theta_r}{\tau} \rangle_{\theta^e} = \frac{-\theta^e + \theta_r}{\tau}, \tag{7}$$

where τ is a relaxation timescale and θ_r is the equilibrium temperature; both are constants for each temperature percentile. This is a linear parameterization of the complex physics contained in $\dot{\theta}$. We separate θ_r into the mean of the temperature distribution and another constant, which we will call the equilibrium temperature anomaly, θ_0: $\theta_r = \theta_{\mathrm{mean}} + \theta_0$. If θ_0 and τ are independent of percentile, this is equivalent to a Newtonian relaxation in the initial temperature advection equation. Our framework will test whether this is a valid assumption.

Substituting equation (7) into equation (6), assuming that the temperature distribution is in steady state ($\frac{\partial \theta^e}{\partial t} = 0$) and rearranging, to first order,
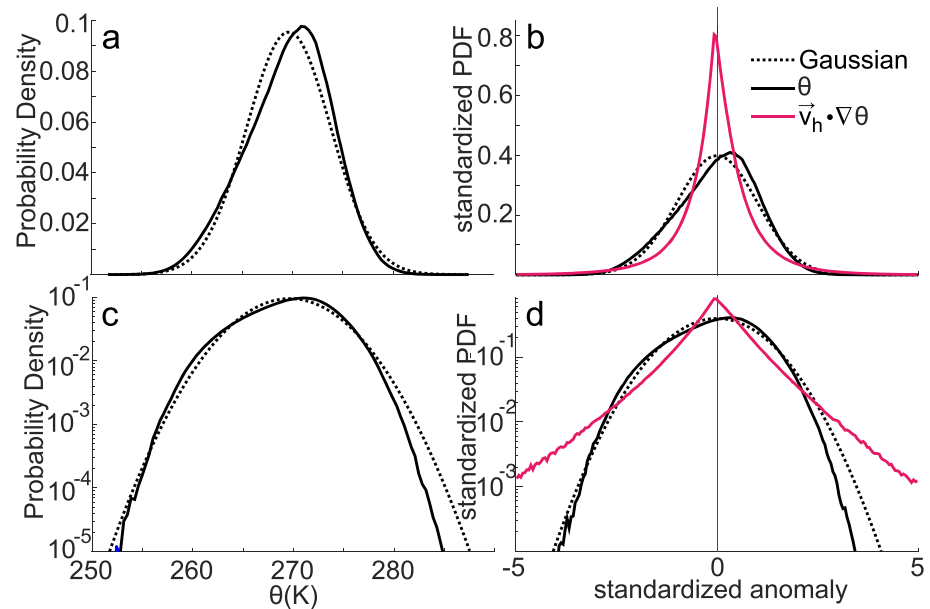
Figure 1. Probability distribution functions at 46° and 837 hPa for the idealized aquaplanet model control run. (a) and (c) Temperature (solid lines) and Gaussian (dotted lines). (b) and (d) Normalized temperature (solid black), temperature advection (solid magenta), and standard Gaussian (dotted black).

$$\theta^e = \theta_{\mathrm{mean}} - \tau \langle \mathbf{v} \cdot \Delta\theta \rangle_{\theta^e} + \theta_0. \tag{8}$$

Thus the temperature of a particular percentile is linearly related to the temperature advection that occurs at that percentile, provided that nonlinear contributions from other processes are small. The mean of the advection of temperature conditional on the percentile of temperature, $-\langle \mathbf{v} \cdot \Delta\theta \rangle_{\theta^e}$, will be referred to henceforth as "conditional temperature advection." The integral of $-\tau \langle \mathbf{v} \cdot \Delta\theta \rangle_{\theta^e} + \theta_0$ over the full distribution of temperature is zero.

In the midlatitudes, a scale analysis would predict horizontal temperature advection to be much stronger than vertical temperature advection. Therefore, we consider the vertical component, $\omega \partial\theta/\partial p$ as part of $\dot{\theta}$ in (1) and let temperature advection be only horizontal: $\mathbf{v} \cdot \Delta\theta = u\partial\theta/\partial x + v\partial\theta/\partial y$. Details of splitting the "other processes" into different components (vertical temperature transport, latent heating, radiation, etc.) is the subject of ongoing work.

We direct the interested reader to an expanded derivation in the supporting information.

3. Idealized Aquaplanet Model With Full Radiative Transfer

We test this framework in an idealized moist general circulation model with a comprehensive radiative transfer code (Paynter & Ramaswamy, 2014) from the Geophysical Fluid Dynamics Laboratory (details in Clark et al., 2018). This aquaplanet model with a 1 m slab ocean has a comprehensive radiative transfer scheme to allow for the water vapor radiation feedback (Paynter & Ramaswamy, 2014). This model includes a simplified Betts-Miller parameterization of convection (Frierson, 2007). Latent heat is released, and when water vapor condenses through large-scale processes or the convection scheme, it rains out instantaneously (Merlis et al., 2013). There are no parameterizations of clouds and no interactively simulated cloud radiative effects. The resolution is 128° longitude by 64° latitude with 30 vertical levels.

The runs are a control run with the mixing ratio of the well-mixed carbon dioxide (CO_2) prescribed to 277 ppm, a doubled CO_2 simulation (CO_2=554ppm), and a quadrupled CO_2 simulation (CO_2 = 1,108 ppm). The temporal resolution of output is 6-hourly, and all calculations are done with 15 years of data (unless specified otherwise), after allowing for a 5-year spin-up time.

The zonal mean zonal wind and temperature mean, variance, and skewness are shown in Figures S1 and S2 in the supporting information. The moments of the distribution are not fully realistic, but they are
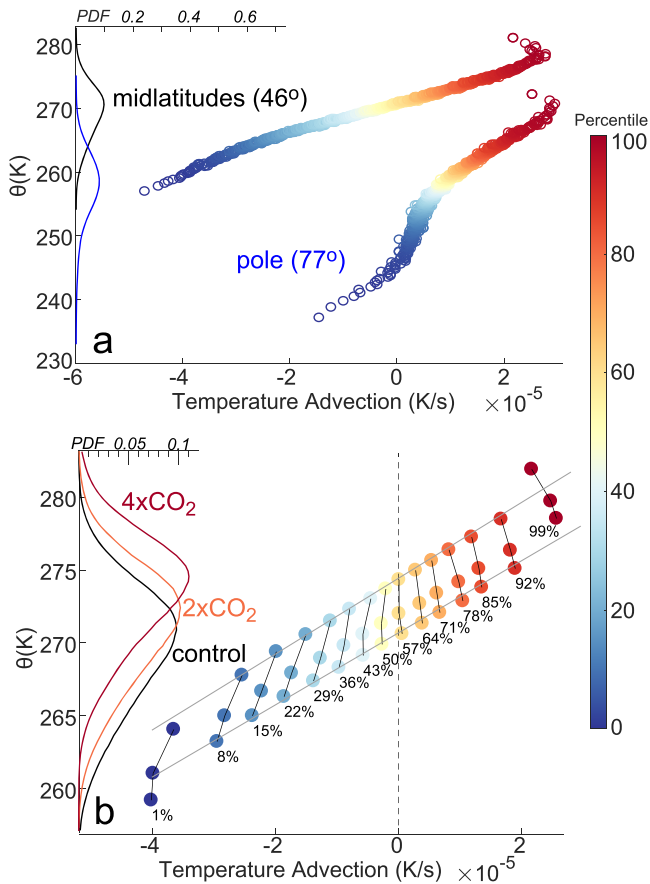
Figure 2. Temperature versus the temperature advection conditionally averaged at each temperature percentile at 837 hPa. (a) Bins are spaced every 0.1% at 46° and 77° in the control run of the model. Corresponding PDFs of temperature are shown in the lines (black and blue, respectively). Percentiles are indicated by the color of the circles. (b) At 46°, bins are spaced every 1% and points are subsampled. The lower set of dots is the control, the middle is the doubled CO_2, and the upper is the quadrupled CO_2 run. Corresponding PDFs of temperature are shown in the lines: black is control, orange is doubled CO_2, and red is quadrupled CO_2. Thin black lines connect the centers of the dots at each percentile as a visual aid. Gray lines are best fit lines to the control and quadrupled CO_2 runs (see equation (8)): $\theta^e = 269.66 - 2.48 \times 10^5 \langle \mathbf{v} \cdot \varDelta\theta \rangle_{\theta^e} + 0.99$ and $\theta^e = 273.54 - 2.61 \times 10^5 \langle \mathbf{v} \cdot \varDelta\theta \rangle_{\theta^e} + 0.86$, respectively. For more discussion, see Supporting Information S1.

significantly non-Gaussian. This model is sufficient to show significant shifts to temperature distributions with increased greenhouse gases.

4. Aquaplanet Temperature Distributions

We calculate the temperature percentiles and the conditional temperature advection at every latitude at 837 hPa for the aquaplanet model. (Other low levels have similar results, but this enables more direct comparison with results of Tamarin-Brodsky et al., 2019, and Garfinkel & Harnik, 2017). We aggregate the identical hemispheres, and the resulting distributions are averaged over all longitudes. Figure 1a shows a midlatitude temperature distribution in the control run. This distribution is non-Gaussian, with its median above the mean. Figure 1c shows the log scale of the probability density, enabling a clear view of the non-Gaussianity. Figures 1b and 1d show the temperature PDF normalized by its standard deviation along with the PDF of the horizontal temperature advection itself. These two quantities have no obvious relationship; the horizontal temperature advection must be averaged at each temperature percentile for the framework to make sense.

The temperature percentiles are plotted against the conditional temperature advection in Figure 2. Figure 2a shows the control run (with 0.2% bins that have 0.1% overlap). Equation (8) decomposes the temperature distribution into the horizontal temperature advection and all other processes, where the linearization of those other properties is expressed as Newtonian relaxation to an equilibrium temperature. If Newtonian relaxation were a complete description of the physics, it would affect each percentile in the same way—τ^e and θ_0^e would be independent of percentile. Therefore, the extent to which the relationship shown in Figure 2 is linear is an indication of the importance of differences of these other processes across percentiles.

In the midlatitudes, the majority of the distribution (∼10–90%) is captured by a single slope (the relaxation time scale, τ) and intercept (the equilibrium temperature, θ_r). At the high latitude, however, the percentiles beneath 40% and above 95% deviate substantially from a simple linear relationship. (Other middle-to-high latitudes are in Figure S3; tropics are in Figure S4.) Where the curvature in the scatterplot of temperature versus temperature advection becomes significant, the simple linear parameterization of Newtonian relaxation is not sufficient, and the details of the diabatic processes matter. The location of the transition from linearity to nonlinearity is a key product of this diagnostic framework, as it identifies the percentiles where the drivers of the temperature distribution change.

To better understand local high-temperature anomalies, we consider the associated horizontal winds and temperature. Figure 3 shows composite maps of temperature and wind fields for the 90th and 99th percentiles (with 1% bins) at the same latitudes. (Tropics are shown in Figure S5; velocities are similar for 90th and 99th percentiles, but the temperature gradient is stronger for the latter.) At the high latitude for the 99th percentile, the wind is transporting air that is the highest temperature anywhere in the domain. The transport cannot increase the temperature further, which means that processes besides horizontal temperature advection (radiation, convection, latent heat release, vertical temperature advection) must be critical for the development of this extreme. In the midlatitudes, the 90th percentile winds are transporting air down a strong temperature gradient, thus having a positive temperature tendency at the location of the anomaly. The 99th percentile shows a wind field mostly aligned with the temperature gradient, so although the winds are significantly stronger than in the 90th percentile, the horizontal temperature advection is as not much
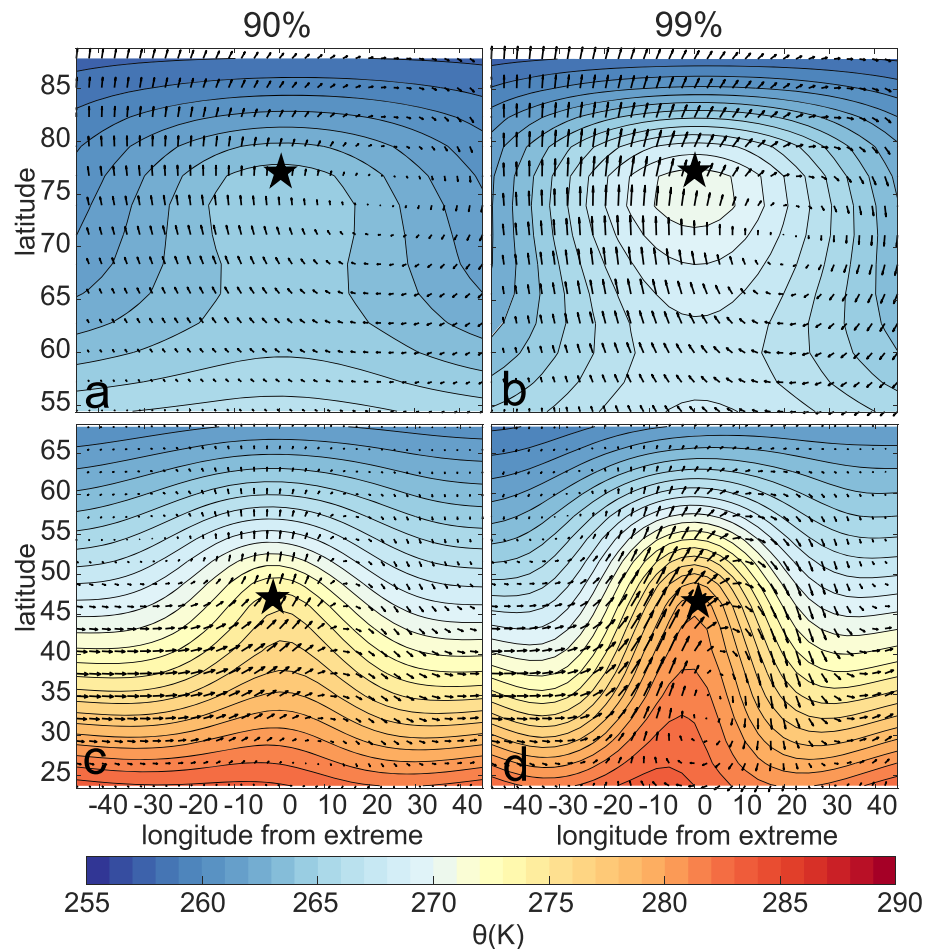
Figure 3. The 837 hPa winds in vectors and temperature in contours (spaced every 1 K) composited around the location indicated by the star at times of (a, c) the 90th percentile and (b, d) the 99th percentile of temperature at (a, b) 77°N and (c, d) 44°N.

stronger. The winds are consistent with a blocking anticyclone and associated summertime midlatitude extreme heat events (Bieli et al., 2015). Cold extremes are shown in Figure S6 in the supporting information.

Next, we consider changes to the temperature distribution in the doubled and quadrupled CO_2 runs. Figure 2b shows the temperature distribution and conditional temperature advection at 46° calculated with 1% bins for the control run, the doubled CO_2 run, and the quadrupled CO_2 run. Thin black lines connecting the percentiles in the different runs are a visual aid for assessing changes: a vertical line indicates a shift only in the temperature of the percentile and no associated change in temperature advection; a horizontal line indicates a shift only in the temperature advection of the percentile with no associated change in temperature. (The latter does not occur, as all percentiles warm with increased CO_2.) Increasing CO_2 shifts the mean of the temperature distribution (at 46° : control = 269.63 K, 2 × CO_2 = 271.13 K, 4 × CO_2 = 273.52 K) and decreases the variance. The change from the control run to the doubled CO_2 run (1.50 K) is not the same as the change from the doubled CO_2 run to the quadrupled CO_2 run (2.39 K). Best fit lines are included for the control run and for the quadrupled CO_2 run. Table S1 reports fits for all three runs, and it demonstrates that the change from the doubled CO_2 run to the quadrupled CO_2 run involves a significant change in the diabatic processes, while the change from the control run to the doubled CO_2 run does not.

Why are the temperature distribution changes for a doubling of CO_2 different for different initial states? Next, we use the framework of the relationship of the conditional temperature advection with the temperature to diagnose the fraction of the temperature change that is due to changes in the mean temperature, in the horizontal advection, and in the other processes.
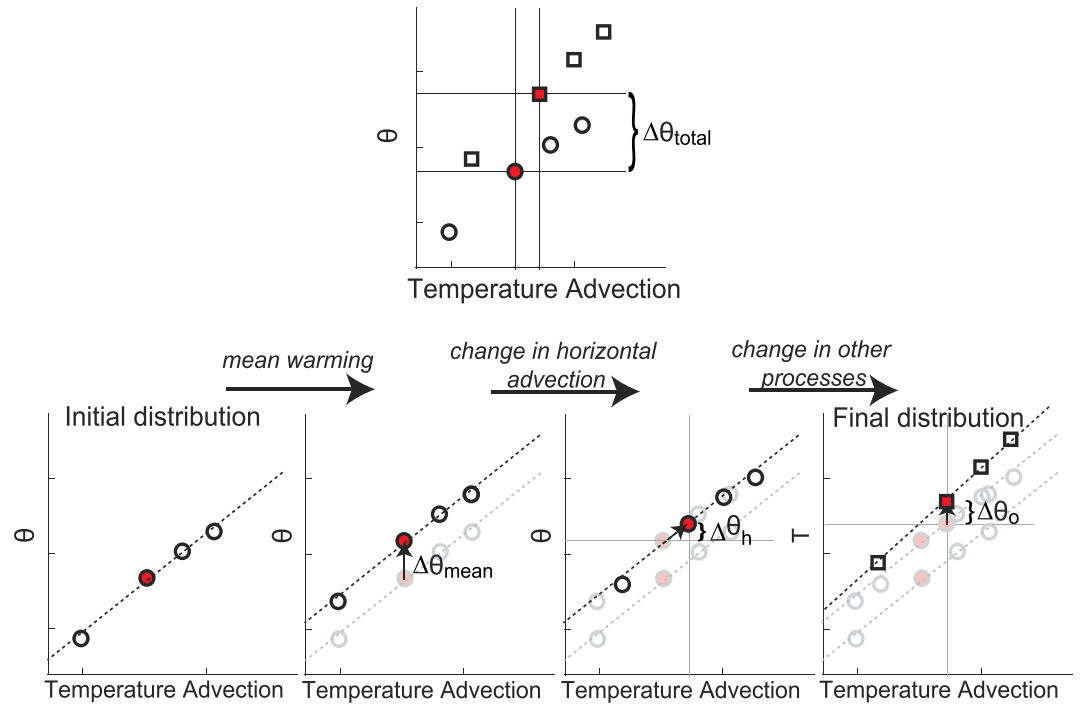
Figure 4. Diagram of decomposition of changes to a temperature distribution into different components. The top panel shows the initial temperature distribution (lower set of dots) and the final, shifted temperature distribution (upper squares), with one point in red. The difference between the initial and final temperature of this red point is $\Delta\theta_{total}$. Lower panels depict a step-by-step decomposition of the shift from the initial temperature distribution to the final temperature distribution. The first panel shows four points in the initial distribution and the local slope for the highlighted red point in the dotted black line. The second panel shows the new distribution associated with uniform warming. The third panel shows the shift associated with a change in the horizontal temperature advection while maintaining the same slope. The final panel shows the change due to changes in the other processes, with the local slope and intercept changing.

5. Decomposition of Change into Horizontal Advection and Other Processes

We decompose the total shift in the temperature at a given percentile, $\Delta\theta_e$, into three components due to: (1) the shift in the mean, (2) differences in the horizontal temperature advection, and (3) changes in other processes. This decomposition is shown schematically in Figure 4. We write

$$\Delta\theta_e = \underbrace{\Delta\theta_{mean}}_{1} \underbrace{- \tau_i \Delta \langle \mathbf{v} \cdot \Delta\theta \rangle_{\theta^e}}_{2} + \underbrace{\Delta\theta_0 - \langle \mathbf{v} \cdot \Delta\theta \rangle_{\theta^e}|_i \Delta\tau - \Delta \langle \mathbf{v} \cdot \Delta\theta \rangle_{\theta^e} \Delta\tau}_{3} \qquad (9)$$

The i subscript indicates the initial distribution. Note that the method is independent of order of operations. The shift in the mean warming is calculated separately and is considered first (Term 1). Next, the change in temperature associated with the difference in conditional temperature advection is calculated as the product of the difference of the conditional temperature advection with the local slope (τ) of the initial distribution (Term 2). This is the case where neither the damping time scale nor the intercept temperature from the linear parameterization change. Finally, there is the component of the temperature change due to the (linearized) other processes (Term 3), which takes the form of a change in the damping timescale and/or the θ_0.

We apply this framework to explore differences in the temperature distributions with doubled CO_2 and quadrupled CO_2. A cubic spline was fit to the data, enabling smooth calculations for the local slope and intercept. Figure 5 shows the normalized shift of temperature percentiles from the control run to the doubled CO_2 run (a) and from the doubled CO_2 run to the quadrupled CO_2 run (b). The black dots show the difference between the change in temperature for each percentile compared to the shift in the mean. Without performing a full decomposition into moments (cf. McKinnon et al., 2016), we can see a decrease in variance in both (a) and (b). Cold percentiles are warmer and warm percentiles colder than from just a shift in the mean of the distribution. For the doubled CO_2, there is a deviation at the lowermost percentile, where the increase
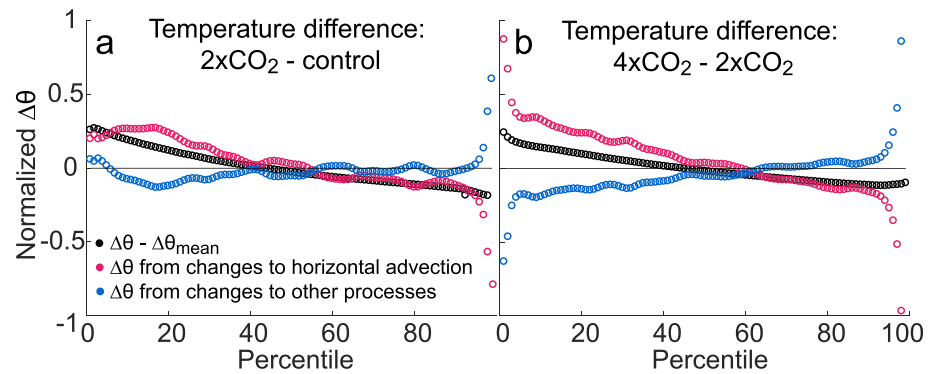
Figure 5. The decomposition of changes in the temperature distribution following the method depicted in Figure 4 and described in section 5 for (a) the doubled CO_2 run compared to the control and (b) the quadrupled CO_2 compared to the doubled CO_2. At each percentile, the temperature change (normalized by the mean temperature difference between the two distributions) is shown. Black: change in temperature at each percentile compared to the change in the mean temperature. Magenta: change due to horizontal temperature advection. Blue: change due to changes in other processes.

in temperature for the 1st percentile is less than that for the 2nd percentile; that implies decreased skewness, as the negative extremes are a bit more extreme. For the quadrupling of CO_2, unlike the change from the initial doubling of CO_2, the skewness increases—both tails are turned upward instead of downward.

The contributions of horizontal advection and of other processes to changes in percentiles are shown in red and blue, respectively. With the doubled CO_2 run, most of the change is due to the temperature advection. Other processes compensate this somewhat in the lower half of the distribution, but they have almost no influence on the change in the upper half. Comparing the quadrupled CO_2 run to the doubled CO_2 run shows a stronger compensation between horizontal temperature advection and other processes. The horizontal temperature advection decreases the variance, while the diabatic processes are increasing variance.

The change in temperature has thus been divided into the components due to changes in the mean of the distribution, in horizontal temperature advection, and in other processes. It can be further subdivided. The conditional temperature advection can be split into the horizontal temperature advection difference due to changes in the gradient of temperature and changes to the winds, for example, or Term 3 of equation (9) can be subdivided.

6. Summary

In this study, we have addressed the question of what sets the shape of temperature distributions using an idealized aquaplanet model. We introduce a framework that relies on averages conditioned on the temperature distribution. In some respects, this approach is standard—looking at composites of meteorological fields during heat waves is common. What is novel is examining the whole temperature distribution with this compositing framework instead of looking at thresholds. We provide a simple interpretation of the budget that enables decomposition of changes to the distribution into different processes: mean warming, horizontal advection, and other processes.

We find that in midlatitudes, the majority of the shape of the distribution is explained by horizontal temperature advection, with the linear parameterization of the other processes constant across percentiles. At the positive tail of the midlatitude distribution and for much of the distribution at high latitudes, differences in the other processes across percentiles are critical for the shape of the distribution. The changes in the distributions associated with doubling and quadrupling CO_2 are not the same; the doubling of CO_2 changes the distribution through the horizontal advection, while quadrupling of CO_2 causes significant changes to diabatic processes. This implies that for smaller changes to the CO_2 burden, a detailed and accurate understanding of the diabatic processes is necessary to understand the tails, but these details become increasingly important for the entire distribution with greater forcing.

We have focused on temperature distributions in this paper, but the framework can be generalized to any other tracer. For example, time-integration would enable analysis of heat waves, precipitation has already

been examined (Chen et al., 2019; Norris et al., 2019), and the framework is promising for examining the changing air pollution.

References

Alexander, L., & Perkins, S. (2013). Debate heating up over changes in climate variability. *Environmental Research Letters*, *8*(4), 41001. https://doi.org/10.1088/1748-9326/8/4/041001

Bieli, M., Pfahl, S., & Wernli, H. (2015). A Lagrangian investigation of hot and cold temperature extremes in Europe. *Quarterly Journal of the Royal Meteorological Society*, *141*(686), 98–108. https://doi.org/10.1002/qj.2339

Chen, G. (2013). The mean meridional circulation of the atmosphere using the mass above isentropes as the vertical coordinate. *Journal of the Atmospheric Sciences*, *70*(7), 2197–2213. https://doi.org/10.1175/JAS-D-12-0239.1

Chen, G., Norris, J., Neelin, J. D., Lu, J., Leung, L. R., & Sakaguchi, K. (2019). Thermodynamic and dynamic mechanisms for hydrological cycle intensification over the full probability distribution of precipitation events. *Journal of the Atmospheric Sciences*, *76*(2), 497–516. https://doi.org/10.1175/JAS-D-18-0067.1

Clark, S. K., Ming, Y., Held, I. M., & Phillipps, P. J. (2018). The role of the water vapor feedback in the ITCZ response to hemispherically asymmetric forcings. *Journal of Climate*, *31*(9), 3659–3678. https://doi.org/10.1175/JCLI-D-17-0723.1

Coumou, D., Lehmann, J., & Beckmann, J. (2015). The weakening summer circulation in the Northern Hemisphere mid-latitudes. *Science*, *348*(6232), 324–327. https://doi.org/10.1126/science.1261768

Frierson, D. M. W. (2007). The dynamics of idealized convection schemes and their effect on the zonally averaged tropical circulation. *Journal of the Atmospheric Sciences*, *64*, 1959–1976. https://doi.org/10.1175/JAS3935.1

Garfinkel, C. I., & Harnik, N. (2017). The non-Gaussianity and spatial asymmetry of temperature extremes relative to the storm track: The role of horizontal advection. *Journal of Climate*, *30*(2), 445–464. https://doi.org/10.1175/JCLI-D-15-0806.1

Harrington, L. J., Frame, D. J., Fischer, E. M., Hawkins, E., Joshi, M., & Jones, C. D. (2016). Poorest countries experience earlier anthropogenic emergence of daily temperature extremes. *Environmental Research Letters*, *11*(5), 55007. https://doi.org/10.1088/1748-9326/11/5/055007

Held, I. M., & Suarez, M. J. (1994). A proposal for the intercomparison of the dynamical cores of atmospheric general circulation models. *Bulletin of the American Meteorological Society*, *75*, 1825–1830. https://doi.org/10.1175/1520-0477(1994)075<1825:APFTIO>2.0.CO;2

Hoskins, B., & Woollings, T. (2015). Persistent extratropical regimes and climate extremes. *Current Climate Change Reports*, *1*(3), 115–124. https://doi.org/10.1007/s40641-015-0020-8

Linz, M., Chen, G., & Hu, Z. (2018). Large-scale atmospheric control on non-Gaussian tails of midlatitude temperature distributions. *Geophysical Research Letters*, *45*, 9141–9149. https://doi.org/10.1029/2018GL079324

Loikith, P. C., & Neelin, J. D. (2015). Short-tailed temperature distributions over North America and implications for future changes in extremes. *Geophysical Research Letters*, *42*, 8577–8585. https://doi.org/10.1002/2015GL065602

Mann, M. E., Rahmstorf, S., Kornhuber, K., Steinman, B. A., Miller, S. K., Petri, S., & Coumou, D. (2018). Projected changes in persistent extreme summer weather events: The role of quasi-resonant amplification. *Science Advances*, *4*(10), eaat3272. https://doi.org/10.1126/sciadv.aat3272

McKinnon, K. A., Rhines, A., Tingley, M. P., & Huybers, P. (2016). The changing shape of Northern Hemisphere summer temperature distributions. *Journal of Geophysical Research: Atmospheres*, *121*, 8849–8868. https://doi.org/10.1002/2016JD025292

Merlis, T. M., Schneider, T., Bordoni, S., & Eisenman, I. (2013). Hadley circulation response to orbital precession. Part I: Aquaplanets. *Journal of Climate*, *26*, 740–753. https://doi.org/10.1175/JCLI-D-11-00716.1

Nakamura, N. (1995). Modified Lagrangian-mean diagnostics of the stratospheric polar vortices. Part I. Formulation and analysis of GFDL SKYHI GCM. *Journal of the Atmospheric Sciences*, *52*(11), 2096–2108.

Norris, J., Chen, G., & Neelin, J. D. (2019). Thermodynamic versus dynamic controls on extreme precipitation in a warming climate from the community earth system model large ensemble. *Journal of Climate*, *32*(4), 1025–1045. https://doi.org/10.1175/JCLI-D-18-0302.1

Paynter, D., & Ramaswamy, V. (2014). Investigating the impact of the shortwave water vapor continuum upon climate simulations using GFDL global models. *Journal of Geophysical Research: Atmospheres*, *119*, 10,720–10,737. https://doi.org/10.1002/2014JD021881

Quinting, J. F., & Reeder, M. J. (2017). Southeastern Australian heat waves from a trajectory viewpoint. *Monthly Weather Review*, *145*(10), 4109–4125. https://doi.org/10.1175/MWR-D-17-0165.1

Rhines, A., McKinnon, K. A., Tingley, M. P., & Huybers, P. (2017). Seasonally resolved distributional trends of North American temperatures show contraction of winter variability. *Journal of Climate*, *30*(3), 1139–1157. https://doi.org/10.1175/JCLI-D-16-0363.1

Seneviratne, S. I., Corti, T., Davin, E. L., Hirschi, M., Jaeger, E. B., Lehner, I., et al. (2010). Investigating soil moisture–climate interactions in a changing climate: A review. *Earth-Science Reviews*, *99*(3), 125–161. https://doi.org/10.1016/j.earscirev.2010.02.004

Tamarin-Brodsky, T., Hodges, K., Hoskins, B. J., & Shepherd, T. G. (2019). A dynamical perspective on atmospheric temperature variability and its response to climate change. *Journal of Climate*, *32*(6), 1707–1724. https://doi.org/10.1175/JCLI-D-18-0462.1

Zschenderlein, P., Fink, A. H., Pfahl, S., & Wernli, H. (2019). Processes determining heat waves across different European climates. *Quarterly Journal of the Royal Meteorological Society*, *145*(724), 2973–2989. https://doi.org/10.1002/qj.3599